Contents lists available at ScienceDirect

Sensors and Actuators A: Physical

A digital light processing 3D printer for fast and high-precision fabrication of soft pneumatic actuators

Lisen Ge [a,b,1], Longteng Dong [a,b,1], Dong Wang [c], Qi Ge [c,d,**], Guoying Gu [a,b,*]

[a] State Key Laboratory of Mechanical System and Vibration, Shanghai Jiao Tong University, Shanghai 200240, China
[b] Robotics Institute, School of Mechanical Engineering, Shanghai Jiao Tong University, Shanghai 200240, China
[c] Digital Manufacturing and Design Center, Singapore University of Technology and Design, Singapore 487372, Singapore
[d] Science and Math Cluster, Singapore University of Technology and Design, Singapore 487372, Singapore

A R T I C L E   I N F O

A B S T R A C T

In this paper, we built up a desktop digital light processing (DLP) 3D printer and fabricated multiple size soft pneumatic actuators integrally with fast speed and high precision. The printing process is based on the projection microstereolithography method. The composition of the printing system and key parameters during the printing process were presented. Evaluation experiments demonstrate that our printer can print objects with as small as 87.5 μm size features. We first printed single pneumatic net-works (pneu-net) actuators integrally and conducted a series of actuation experiments and finite element method analyses to test the actuators' deformation capability. We further designed a soft pneumatic gripper containing three micro pneu-net actuators with 0.4 mm wide square air channels as well as 0.2 mm thick chamber walls and fabricated the gripper integrally in less than 30 min using our printer. The grasping capability of the gripper was verified through experiments as well. Results presented in this work prove the performance of the DLP printer we build up and show the convenience of fabricating micro soft pneumatic actuators integrally using DLP 3D printing approach with fast speed and high precision.

© 2018 Elsevier B.V. All rights reserved.

1. Introduction

Soft Robotics, especially soft pneumatic robotics as an emerging field has achieved rapid progress in recent years [1]. Previous studies have indicated that soft pneumatic actuators (SPAs) can generate various type of deformations, such as extension, expanding, bending and twisting and a combination of them [2,3]. Using SPAs could realize different kinds of motions, such as creeping [4,5], rotating [6], rolling [7], and jumping [8]. Novel soft grippers [9] and soft hands [10] based on SPAs have also been delivered to conduct manipulating tasks. Due to the soft nature, efforts have also been made to employ the micro-SPAs as micro-manipulators in the field of medicine such as minimally invasive surgery [11–13], where sub-millimeter size features are generally necessary.

To design and investigate the SPAs, fabrication techniques are very important. Currently, the molding technique is commonly uti-

lized [12–17]. As shown in Fig. 1(a), this technique is generally time-consuming and requires cumbersome fabrication processes. For instance, manufacturing a pneumatic networks (pneu-net) actuator [18] with the molding approach requires multi-steps and needs extra bonding processes (Fig. 1(a)). More importantly, the fabrication scale and the structure variety are also limited by the molds. Fabricating micro-SPAs with complicated inner structure features using the molding approach is greatly challenging if not impossible. To address this problem, some modified methods [11,19] are developed to eliminate the use of molds and simplify the manufacturing process. However, multi-steps are still necessary and the structures of the fabricated actuators are relatively simple. Alternatively, 3D printing is promising to solve this problem by fabricating the structure directly. During the past decade, different 3D printing methods such as selective laser sintering (SLS) [20], fused deposition modeling (FDM) [21–23], fused filament fabrication (FFF) [24] have been employed. Although the fabricated SPAs exhibit good mechanical performance, the resolution and surface quality are relatively low [25]. On the other hand, the digital light processing (DLP) method based on projection microstereolithography technique selectively solidifies the liquid photocurable resin layer-by-layer, where each layer can be cured entirely at one time in seconds and no additional supporting structure is required [25].

---

* Corresponding author at: State Key Laboratory of Mechanical System and Vibration, Shanghai Jiao Tong University, Shanghai 200240, China.
** Corresponding author at: Digital Manufacturing and Design Center, Singapore University of Technology and Design, Singapore 487372, Singapore.
E-mail addresses: ge_qi@sutd.edu.sg (Q. Ge), guguoying@sjtu.edu.cn (G. Gu).
[1] These authors contribute equally to the current work.
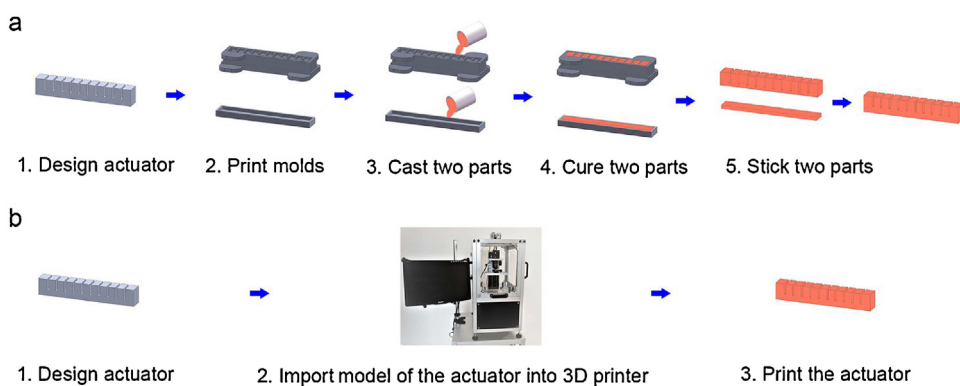
Fig. 1. Main procedure of fabricating a pneu-actuator through (a) molding approach; and (b) 3D printing method.

This leads to the advantages of the high resolution and high surface quality [26–34]. With such DLP 3D printing method, many efforts have been recently attempted to fabricate SPAs. They generally focus on the investigation of the material properties [26–29], such as rheology behavior [26,27,29], tensile elongations [27–29], tunable mechanical behavior [27–29], self-healing behavior [27] and multi-material printing performance [29]. The manufacturing scales in their works are usually millimeter or larger. To the best of our knowledge, the DLP 3D printing method has not been well studied to fabricate micro-SPAs that typically contain sub-millimeter scale features. In this paper, we design a DLP 3D printer and present a systemic study for fast and high-precision fabrication of the SPAs with complex inner structure and sub-millimeter scale features.

We first reported the method of building up a bottom-up DLP 3D printer with a resolution of 50 μm based on projection microstereolithography technique [32]. Using Tangoplus FLX 930 (Stratasys) as photocurable elastomer and Rhodamine B (Acros Organics) as photo absorber, we printed the Shanghai Jiao Tong University (SJTU) badges of different sizes to evaluate the minimum printable scale of our printer. Results indicate that our printer can fabricate objects with features as small as 87.5 μm. Next, we presented a straightforward approach to directly 3D print pneu-net actuators exhibiting large deformation. Actuation experiments and FEM analyses indicate that the printed pneu-net actuator can generate sufficient large deformations under 20 kPa input air pressure. Finally, we introduced the design and fabrication of a micro soft pneumatic gripper consisting of scaled-down pneu-net actuators with 0.4 mm wide square air channels as well as 0.2 mm thick chamber walls respectively. Experiments were conducted to verify the grasping capability of the DLP printed gripper.

2. Materials and methods

2.1. DLP printing system setup

DLP printing is a fast additive manufacturing method with high resolution. The working principle of this approach has been detailed in Refs. [30,35,36] and is briefly summarized here.

As shown in Fig. 2(a), the 3D geometry model of an object is first sliced into layers horizontally. The thin layers are then converted into 2D mask images. A light projection device is employed to cure the photopolymer resin. It uses a digital masking technique to project a dynamically defined mask image onto the resin surface of each layer. According to Ref. [30], a bottom-up projection system has many advantages compared to a top-bottom system. In a bottom-up projection system, the mask image is projected onto the bottom of the resin tank and the newly cured resin adheres to the tank bottom and the cured part simultaneously. After one layer is cured, the platform is first lifted up to separate the cured layer from the tank bottom and then driven down to form a gap with the tank to cure the next layer. The process is repeated until the whole object is fabricated.

We built up a bottom-up DLP printing system as demonstrated in Fig. 2(b). A DLP projector (Wintech PRO6500) is equipped to provide a 385 nm ultraviolet (UV) light source. The contrast ratio of the projector is 1000:1. The resolution is 1920 × 1080 and the projection area is 96 × 54 mm. The normal resolution is, therefore, 50 μm. According to [35], the digital masking technology mainly consists of three types: liquid crystal display (LCD), digital micro-mirror device (DMD) and liquid crystal on silicon (LcoS). In our development, the projector employs the DMD technique. A customized optical reflector (giai) is used to adjust the direction of the UV light. An electric
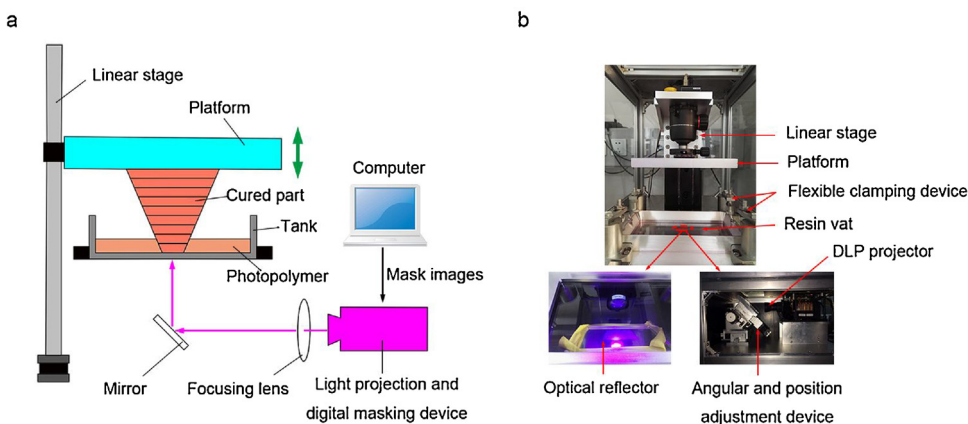

Fig. 2. (a) The schematic of bottom-up DLP printing process. (b) The DLP printing system built up in this work.

angular and position adjusting device (Chuo precision industrial co. ltd, ATS-920-HP) is used to adjust the position and attitude of the optical reflector. The adjustable angle range is $\pm10°$ and the accuracy is 0.002°. The resin vat is with an optical quartz glass bottom and Aluminum alloy frame. A Teflon membrane is coated on the surface of the quartz glass to reduce the separation force between the cured part and the vat bottom [30]. A flexible clamping device is employed to compress the resin vat. This device allows the vat to be lifted a certain height. The compression force that the device applies to the vat increases as the lifting height rises to avoid impact forces. An Aluminum alloy platform is served as a curing bed for the resin. A linear stage (Thorlabs, LTS150M) is employed to drive the platform. The positioning accuracy of the stage is 5 μm. Creation Workshop (Envision Labs) is used to slice the 3D geometry of the objects.

2.2. Materials for printing

Currently, only a few number of photocurable elastomers are commercially available, including EPU 40 (Carbon), Tangoplus (Stratasys), Formlab Flexible (Formlab), and Spot-E Elastic (Spot-A Materials) [28]. Among them, the Tangoplus FLX930 (Stratasys) has the highest elongation at break, which is 170%–220% [37]. Therefore, in this study, we chose Tangoplus FLX930 as an illustration in the following development. It should be noted that all the other photocurable elastomers can also be selected to fabricate the SPAs with the developed DLP 3D printer, while the printing parameters should be determined based on different materials. The readers may refer to [35,38–40] for more detailed explanations.

In addition to the photocurable resin, Rhodamine B (Acros Organics) was introduced as photo absorber. The mass ratio of the photo absorber and the resin should not be either too low to cause overgrowth or too high to cause undercure of the resin. In this work, we set the mass ratio of the photo absorber and the resin as 3:1000.

After Rhodamine B and Tangoplus are mixed up, a mixing process is then conducted at 2000 RPM for 1 min using a planetary centrifugal vacuum mixer (THINKY ARE-310). No further steps are required before the well-mixed materials are applied to printing tasks.

2.3. The complete printing process

The flow chart of the printing process is shown in Fig. 3. After the CAD model of an object is sliced and converted into mask images, the DLP printer is turned on and the images are loaded into the control system of the printer. The printer starts to run after the material is poured into the resin vat. The object is then printed layer by layer.

At the beginning of printing the first layer, the platform is driven down to form a gap with the bottom of the resin tank. The position of the platform should be properly set so that the first layer can be separated from the tank bottom and stay on the platform firmly after being pulled off the tank bottom. After the curing process of the first layer, the printing process is paused and the current position of the platform is recorded. The platform is then lifted up to detect whether the cured layer can be separated from the resin tank bottom. Once the separation problem occurs, the platform is first separated from the tank bottom manually and the cured material is cleared. Then the zero position of the platform is recalibrated, after which the platform is located upper than last trial to form a larger gap for reducing the separation force. The printing process and detection is repeated. After the problem is eliminated, the platform is lifted up to zero to detect whether the cured layer completely stays on the platform after being pulled off the tank bottom. If not, the cured material is cleared. The platform is driven down closer to the tank bottom and the first layer is reprinted. When the
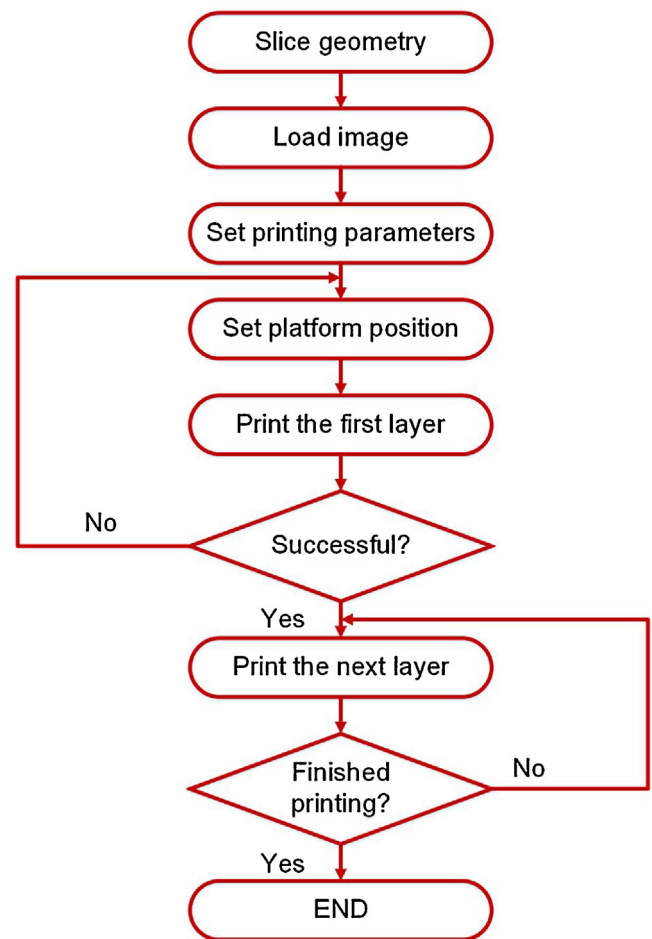

Fig. 3. The flow chart of the DLP printing process.

first layer is successfully printed, the platform is driven down to the recorded position and the rest layers are printed automatically.

During the printing process, several printing parameters can significantly influence the print quality, such as the layer thickness (H_T), the light intensity (I_L) and the curing time (T_C) of each layer. The specific value for each parameter deeply depends on the printing material. In this work, we set $H_T = 50$ μm and $T_C = 4$ s. The brightness of the DLP projector is 1100 mW @ 385 nm. While printing the first layer, I_L is set as 60% of the brightness to ensure the layer adhere to the platform firmly. As for the rest layers, I_L is set as 10% of the brightness.

3. Results and discussion

3.1. Evaluation of fabrication scale of the DLP printer

To evaluate the fabrication scale of our DLP printer, we printed the SJTU badge of different sizes. As shown in Fig. 4(a), the badge is with a 41 mm outer diameter and contains numerous tiny and complicated features. The minimum feature is a rectangle with its short side as 0.35 mm. We define this feature as the basis of assessment. We printed badges with three different sizes (original size, 0.5 times the original size and 0.25 times the original size) along Z-axis. We number them as badge 1, badge 2 and badge 3 respectively. The short side of the minimum feature of each badge is 0.35 mm, 0.175 mm, and 27.5 μm, respectively. By checking whether the minimum feature is successfully printed, we could evaluate the fabrication scale of the printer.
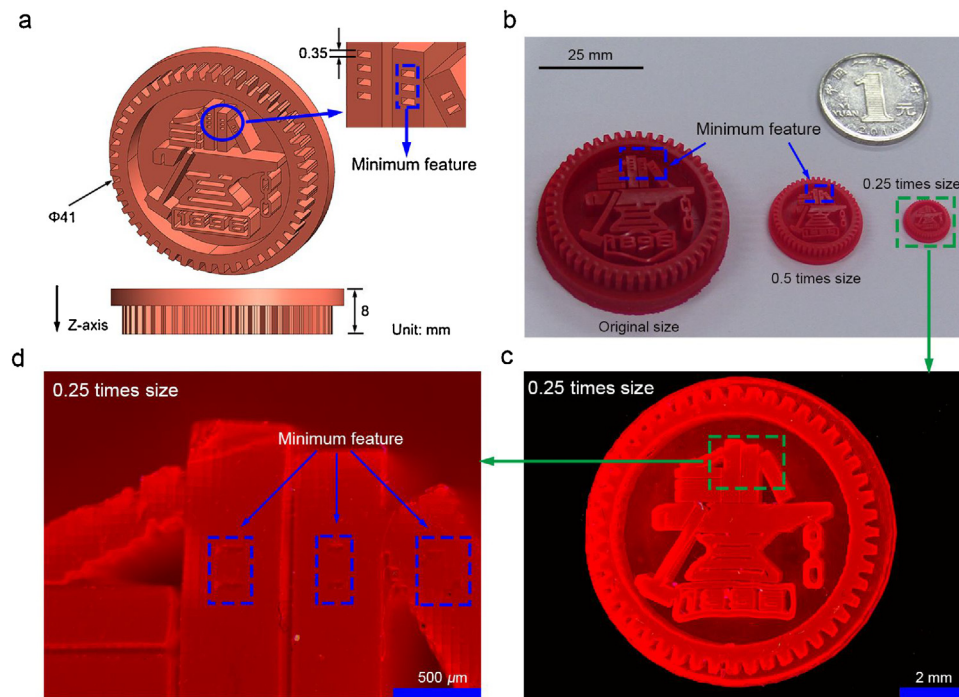
Fig. 4. (a) The geometry model of the SJTU badge; (b) The printed original size badge, 0.5 times size badge and 0.25 times size badge; (c), (d) The microscope photographs of the 0.25 times size badge.

As shown in Fig. 4(b), badge 1 and badge 2 are printed with good quality, neglecting the buckling in some thin-walled features. The minimum features of badge 1 and badge 2 are successfully printed. We took the microscope photographs of badge 3 to check the print quality. As shown in Fig. 4(c) and (d), both the whole body and the minimum feature of badge 3 are successfully printed. We can conclude that our DLP printer can reduce the fabrication scale down to 87.5 μm, which is very close to the DLP projector's resolution (50 μm).

3.2. DLP printing and characterization of single pneu-net actuators

We conducted a series of actuation experiments on the SPAs we printed to evaluate their deformation capability.

Since we introduced Rhodamine B into Tangoplus FLX 930 as photo absorber, we first conducted a uniaxial tensile test using Zwick/Roell Z0020 to evaluate the mechanical property of the printing material. The tensile test is based on standard ASTM D412. The specimens were printed using our DLP printer. Fig. 5(a) demon-

strates the printed specimen and the printing direction (Z-axis). The narrow portion of the specimen is with a length of 33 mm and a width of 6 mm. The thickness of the specimen is 2 mm. The uniform rate of grip separation is 10 mm/min. Three specimens were tested. The stress-strain curve of one specimen is demonstrated in Fig. 5(b). The ultimate strain of the curved material can reach approximately 0.9 and the corresponding stress is about 0.26 MPa. We used the Neo-Hookean model to establish the constitutive equation of the printing material. The stress-strain data of the tensile test was loaded into ABAQUS 6.14-4 (Dassault Systemes S.A) to evaluate the constitutive parameters. All the three specimens were evaluated and the average values of the Neo-Hookean model parameters were $C_{10} = 0.067$, $D_1 = 0$.

Considering the relatively low ultimate strain of the printing material, we selected pneu-net actuators as the test SPAs as they could generate large deformations under relatively low pressures [18]. We first printed normal size pneu-net actuators using our DLP printer. The printed actuator is 0.7 times size of the original actuator in [41]. The bottom of the actuator was thickened to replace the inextensible layer. The printing process is less than
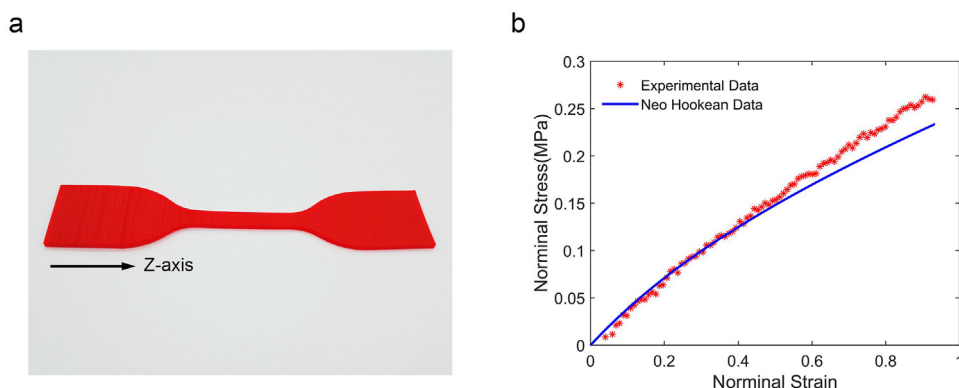

Fig. 5. (a) A tensile test specimen as printed; (b) Stress-strain curve based on tensile test data and Neo-Hookean model fitting data for one specimen.
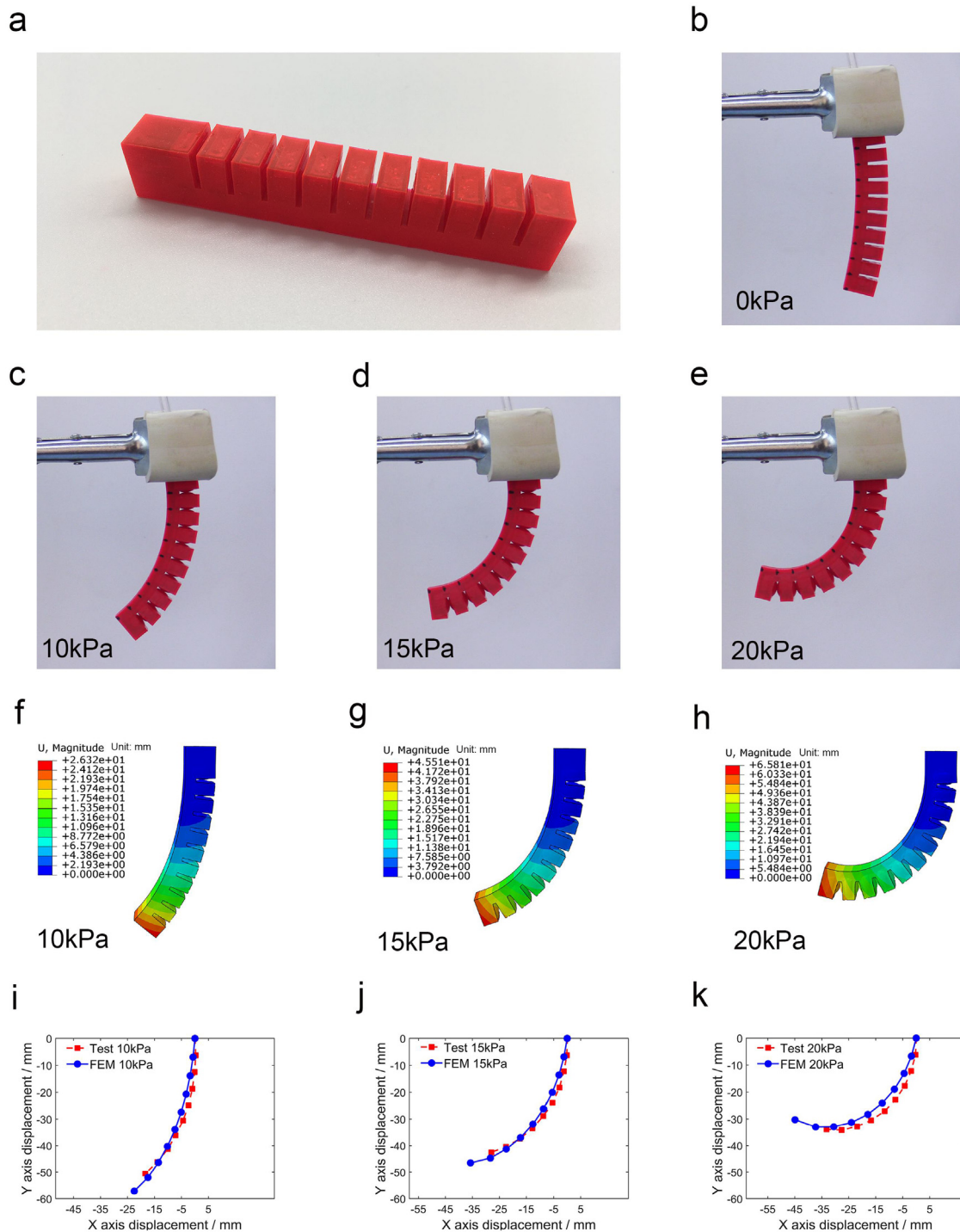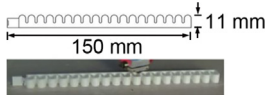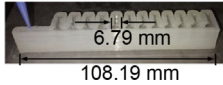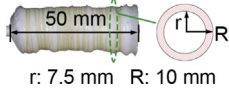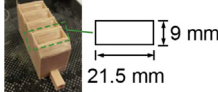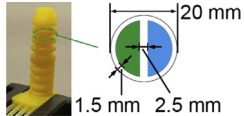
Fig. 6. (a) A printed 0.7 times of the original size pneu-net actuator with good surface quality; (b)–(e) Actuation experiment of the pneu-net actuator under inputting air pressure of 0 kPa, 10 kPa, 15 kPa, 20 kPa; (f)–(h) FEM results of the pneu-net actuator's deformation under inputting air pressure of 10 kPa, 15 kPa, 20 kPa; (i)–(k) Comparison 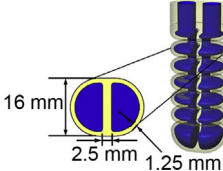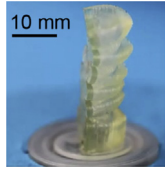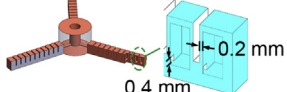of experimental and FEM results of the deformations of markers on the bottom side of the pneu-net actuator under inputting air pressure of 10 kPa, 15 kPa, 20 kPa.

an hour. As shown in Fig. 6(a), the printed actuator has good surface quality. We then conducted a series of actuation experiments to test the deformation capability of the printed actuator. We recorded the complete actuation process and captured the actuator's deformation under different pressures (see Video 1). Fig. 6(b)–(e) demonstrates the deformation of the actuator under 0 kPa, 10 kPa, 15 kPa, and 20 kPa pressure respectively. To verify the experimental results, we conducted a series of finite element method (FEM) analyses based on ABAQUS 6.14-4 (Dassault Sys-

temes S.A) with the aforementioned constitutive parameters. FEM results of the actuator's deformation under different pressures are demonstrated in Fig. 6(f)–(h). We further compared the experimental and FEM results of the deformed profile of the actuator's bottom line under different pressure. The deformed profile of this line is represented by a series of equally spaced points marked on the deformed curve. The positions of these points in the experiments were acquired through ImageJ (National Institutes of Health, USA). Experimental tests were conducted three times and the aver-

Table 1
The state-of-the-art of 3D printing SPAs in the literature.

Technique	Printed SPA	Technique	Printed SPA
SLS [20]	10 mm	FDM [21]	11 mm / 150 mm
FDM [22]	6.79 mm / 108.19 mm	FDM [23]	50 mm / r: 7.5 mm R: 10 mm
FFF [24]	9 mm / 21.5 mm	DLP [26]	20 mm / 1.5 mm 2.5 mm
DLP [27]	16 mm / 2.5 mm 1.25 mm	DLP [28]	10 mm
DLP [29]	d = 38 mm	This paper	0.2 mm / 0.4 mm

a) The feature size information of the printed SPA was acquired from the corresponding author in Ref. [28].

age values were used to compare with FEM results as shown in Fig. 6(i)–(k). It indicates that the experimental results match the FEM results. Moreover, the printed pneu-net actuators can generate sufficient large deformation under relatively low air pressure. We therefore selected pneu-net actuators as the soft pneumatic gripper's actuators.

3.3. DLP printing of a micro soft pneumatic gripper

Interests in miniaturization of SPAs are growing to satisfy the requirement of micro manipulations in minimally invasive surgeries, where micro-SPAs with submillimeter size features are generally necessary. However, the multi-step molding fabricating
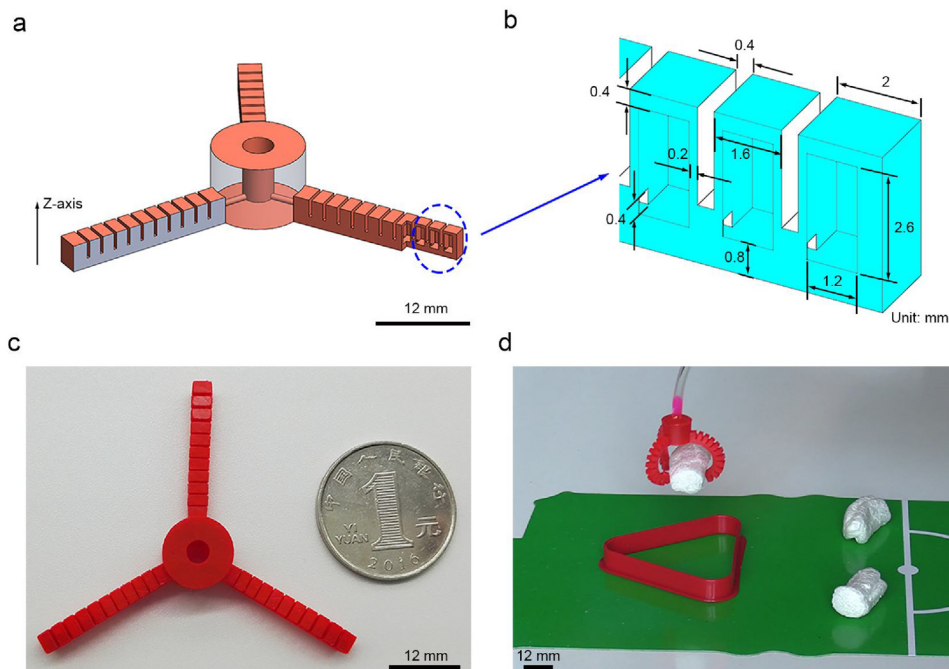

Fig. 7. (a) The 3D CAD model of the designed gripper; (b) The specific dimensions of the pneu-net actuator chambers of the gripper; (c) The DLP printed gripper, with good surface quality; (d) Grasping experiment of the DLP printed gripper.

approach relies on manual operations and becomes challenging while the manufacturing scale is reduced down. Different 3D printing techniques have been introduced to solve this problem by fabricating SPAs directly, as summarized in Table 1.

We can see from Table 1 that since the resolution and surface quality of SLS [20], FDM [21–23] and FFF [24] based methods are relatively low [25], the fabricating scales in these works are millimeter or larger. The DLP technique is characterized by its high resolution and surface quality, while current works [26–29] mainly focus on the investigation of the material properties and their fabrication scales are also millimeter or larger. To investigate the feasibility of fabricating micro-SPAs with submillimeter size features using DLP 3D printing technique, we designed a micro soft pneumatic gripper with 0.4 mm wide square air channels as well as 0.2 mm thick chamber walls and printed the gripper integrally using our DLP printer.

Considering the rectangular projection area of the DLP projector, we designed a three-claw gripper, as shown in Fig. 7(a). The three claws are equally angular distributed and connected to one common inlet air channel. To assure the deformability, the top part of the actuator for each claw is defined as the 0.2 times size of the original pneu-net actuator in [41]. The bottom part of the actuator for each claw is thickened to replace the inextensible layer. The detailed dimensions of the gripper are demonstrated in Fig. 7(b).

The whole body of the gripper was printed using our DLP printer integrally along Z-axis (Fig. 7(a)) in less than 30 min. As demonstrated in Fig. 7(c), the printed gripper is with good surface quality. In addition, since the gripper was fabricated all in one, post-bonding processes and leakage problems at the bonding areas could be eliminated. We conducted an experiment to verify the grasping capability of the gripper. Fig. 7(d) shows the gripper is grasping and transporting an object (The mass of the gripper and the object is 2 g and 0.2 g, respectively. The complete grasping experiment is demonstrated in Video 2). Results indicate that with our self-built-up DLP printer, we can fabricate micro-SPAs that contains submillimeter size features with fast speed and high quality. More importantly, the fabricating process is significantly simplified compared with the molding approach, since the three-claw micro gripper is integrally printed and the bonding processes are avoided. Compared with the current works based on DLP technique as summarized in Table 1, we have successfully reduced the fabrication scale from millimeter down to submillimeter and verified the feasibility of 3D printing micro-SPAs with submillimeter size features using this technique.

4. Conclusions

Based on projection microstereolithography method, we have built up a bottom-up DLP 3D printer and employed the printer to fabricate SPAs and micro soft pneumatic grippers with fast speed and high precision. Evaluations of the printable scale of our DLP printer have been conducted first and it indicates that our printer can fabricate 87.5 μm size structures. Experiments and FEM results prove that the DLP printed pneu-net actuator can generate sufficiently large actuating deformations under relatively low pressure and hence pneu-net actuators are chosen as the gripper's actuators. Finally, a micro soft pneumatic gripper with 0.4 mm wide square air channels as well as 0.2 mm thick chamber walls was printed integrally using our DLP printer in less than 30 min. The printed gripper was with good surface quality and its grasping capability was verified through experiments.

Results in this work have demonstrated the good performance of our DLP printer and the convenience of using DLP 3D additive manufacturing method to fabricate SPAs and micro-SPAs integrally with high efficiency and high precision. Future work includes (1) improving the resolution of the DLP projector to print smaller size features (2) improving the mechanical behavior of the printing material to improve the performance of the printed SPAs (3) realizing the automatic detection of whether the first layer is successfully cured and adjust the position of the platform correspondingly in the printing process with the force sensing.

Conflicts of interest

None.

Appendix A. Supplementary data

Supplementary material related to this article can be found, in the online version, at doi:https://doi.org/10.1016/j.sna.2018.02. 041.

References

[1] L. Hines, K. Petersen, G.Z. Lum, M. Sitti, Soft actuators for small-scale robotics, Adv. Mater. 29 (2017) 1603483, http://dx.doi.org/10.1002/adma.201603483.

[2] F. Connolly, P. Polygerinos, C.J. Walsh, K. Bertoldi, Mechanical programming of soft actuators by varying fiber angle, Soft Rob. 2 (1) (2015) 26–32, http://dx. doi.org/10.1089/soro.2015.0001.

[3] F. Connolly, C.J. Walsh, K. Bertoldi, Automatic design of fiber-reinforced soft actuators for trajectory matching, Proc. Natl. Acad. Sci. U. S. A. 114 (1) (2017) 51–56, http://dx.doi.org/10.1073/pnas.1615140114.

[4] R.F. Shepherd, F. Ilievski, W. Choi, S.A. Morin, A.A. Stokes, A.D. Mazzeo, et al., Multigait soft robot, Proc. Natl. Acad. Sci. U. S. A. 108 (51) (2011) 20400–20403, http://dx.doi.org/10.1073/pnas.1116564108.

[5] M.T. Tolley, R.F. Shepherd, B. Mosadegh, K.C. Galloway, M. Wehner, M. Karpelson, et al., A resilient, untethered soft robot, Soft Rob. 1 (3) (2014) 213–223, http://dx.doi.org/10.1089/soro.2014.0008.

[6] A. Ainla, M.S. Verma, D. Yang, G.M. Whitesides, Soft, rotating pneumatic actuator, Soft Rob. 4 (3) (2017) 297–304, http://dx.doi.org/10.1089/soro.2017. 0017.

[7] M.A. Robertson, J. Paik, New soft robots really suck: vacuum-powered systems empower diverse capabilities, Sci. Rob. 2 (9) (2017) eaan6357, http:// dx.doi.org/10.1126/scirobotics.aan6357.

[8] N.W. Bartlett, M.T. Tolley, J.T.B. Overvelde, et al., A 3D-printed, functionally graded soft robot powered by combustion, Science 349 (6244) (2015) 161–165, http://dx.doi.org/10.1126/science.aab0129.

[9] K.C. Galloway, K.P. Becker, B. Phillips, J. Kirby, S. Licht, D. Tchernov, et al., Soft robotic grippers for biological sampling on deep reefs, Soft Rob. 3 (1) (2016) 23–33, http://dx.doi.org/10.1089/soro.2015.0019.

[10] R. Deimel, O. Brock, A novel type of compliant and underactuated robotic hand for dexterous grasping, Int. J. Rob. Res. 35 (1-3) (2016) 161–185, http:// dx.doi.org/10.1177/0278364915592961.

[11] X. Liang, Y. Sun, H. Ren, A flexible fabrication approach toward the shape engineering of microscale soft pneumatic actuators, IEEE Rob. Autom. Lett. 2 (1) (2017) 165–170, http://dx.doi.org/10.1109/LRA.2016.2585298.

[12] B. Gorissen, W. Vincentie, F. Al-Bender, D. Reynaerts, M. De Volder, Modeling and bonding-free fabrication of flexible fluidic microactuators with a bending motion, J. Micromech. Microeng. 23 (4) (2013) 045012, http://dx.doi.org/10. 1088/0960-1317/23/4/045012.

[13] Y. Sun, S. Song, X. Liang, et al., A miniature soft robotic manipulator based on novel fabrication methods, IEEE Rob. Autom. Lett. 1 (2) (2016) 617–623, http://dx.doi.org/10.1109/LRA.2016.2521889.

[14] S. Wakimoto, K. Suzumori, K. Ogura, Miniature pneumatic curling rubber actuator generating bidirectional motion with one air-supply tube, Adv. Rob. 25 (9–10) (2011) 1311–1330, http://dx.doi.org/10.1163/016918611X574731.

[15] O.C. Jeong, S. Konishi, All PDMS pneumatic microfinger with bidirectional motion and its application, J. Microelectromech. Syst. 15 (4) (2006) 896–903, http://dx.doi.org/10.1109/JMEMS.2006.879377.

[16] B. Gorissen, T. Chishiro, S. Shimomura, D. Reynaerts, M. De Volder, S. Konishi, Flexible pneumatic twisting actuators and their application to tilting

micromirrors, Sens. Actuators A: Phys. 216 (2014) 426–431, http://dx.doi.org/10.1016/j.sna.2014.01.015.

[17] Y. Sun, H. Ren, Soft transnasal endoscopic robot for patient-administered nasopharynx inspection, J. Med. Dev. 9 (2015) 020930, http://dx.doi.org/10.1115/1.4030141.

[18] B. Mosadegh, P. Polygerinos, C. Keplinger, S. Wennstedt, R.F. Shepherd, U. Gupta, et al., soft robotics: pneumatic networks for soft robotics that actuate rapidly, Adv. Funct. Mater. 24 (2014) 2163–2170, http://dx.doi.org/10.1002/adfm.201303288.

[19] J. Paek, I. Cho, J. Kim, Microrobotic tentacles with spiral bending capability based on shape-engineered elastomeric microtubes, Sci. Rep. 5 (2015) 10768, http://dx.doi.org/10.1038/srep10768.

[20] R.B.N. Scharff, E.L. Doubrovski, W.A. Poelman, P.P. Jonker, C.C.L. Wang, J.M.P. Geraedts, Towards behavior design of a 3D-printed soft robotic hand, in: Soft Robotics: Trends, Applications and Challenges, Springer International Publishing, 2017, pp. 23–29, http://dx.doi.org/10.1007/978-3-319-46460-2_4.

[21] H.K. Yap, H.Y. Ng, C.-H. Yeow, High-force soft printable pneumatics for soft robotic applications, Soft Rob. 3 (3) (2016) 144–158, http://dx.doi.org/10.1089/soro.2016.0030.

[22] J. Plott, A. Shih, The extrusion-based additive manufacturing of moisture-cured silicone elastomer with minimal void for pneumatic actuators, Addit. Manuf. 17 (2017) 1–14, http://dx.doi.org/10.1016/j.addma.2017.06.009.

[23] J. Morrow, S. Hemleben, Y. Menguc, Directly fabricating soft robotic actuators with an open-source 3-D printer, IEEE Rob. Autom. Lett. 2 (1) (2017) 277–281, http://dx.doi.org/10.1109/LRA.2016.2598601.

[24] H.M.C.M. Anver, R. Mutlu, G. Alici, 3D printing of a thin-wall soft and monolithic gripper using fused filament fabrication, IEEE, 2017 IEEE International Conference on Advanced Intelligent Mechatronics (AIM) (2017) 442–447, http://dx.doi.org/10.1109/AIM.2017.8014057.

[25] S.C. Ligon, R. Liska, J. Stampfl, M. Gurr, R. Mulhaupt, Polymers for 3D printing and customized additive manufacturing, Chem. Rev. 117 (15) (2017) 10212–10290, http://dx.doi.org/10.1021/acs.chemrev.7b00074.

[26] B.N. Peele, T.J. Wallin, H. Zhao, R.F. Shepherd, 3D printing antagonistic systems of artificial muscle using projection stereolithography, Bioinspir. Biomim. 10 (5) (2015) 055003, http://dx.doi.org/10.1088/1748-3190/10/5/055003.

[27] T.J. Wallin, J.H. Pikul, S. Bodkhe, B.N. Peele, B.C. Mac Murray, D. Therriault, et al., Click chemistry stereolithography for soft robots that self-heal, J. Mater. Chem. B 5 (31) (2017) 6249–6255, http://dx.doi.org/10.1039/C7TB01605K.

[28] D.K. Patel, A.H. Sakhaei, M. Layani, B. Zhang, Q. Ge, S. Magdassi, Highly stretchable and UV curable elastomers for digital light processing based 3D printing, Adv. Mater. 29 (2017) 1606000, http://dx.doi.org/10.1002/adma.201606000.

[29] C.J. Thrasher, J.J. Schwartz, A.J. Boydston, Modular elastomer photoresins for digital light processing additive manufacturing, ACS Appl. Mater. Interfaces 9 (2017) 39708–39716, http://dx.doi.org/10.1021/acsami.7b13909.

[30] Y. Pan, C. Zhou, Y. Chen, A fast mask projection stereolithography process for fabricating digital models in minutes, J. Manuf. Sci. Eng. 134 (5) (2012) 051011, http://dx.doi.org/10.1115/1.4007465.

[31] J. Torgersen, A. Ovsianikov, V. Mironov, N. Pucher, X. Qin, Z. Li, et al., Photo-sensitive hydrogels for three-dimensional laser microfabrication in the presence of whole organisms, J. Biomed. Opt. 17 (10) (2012) 105008, http://dx.doi.org/10.1117/1.JBO.17.10.105008.

[32] X. Zheng, H. Lee, T.H. Weisgraber, M. Shusteff, J. DeOtte, E.B. Duoss, et al., Ultralight, ultrastiff mechanical metamaterials, Science 344 (6190) (2014) 1373–1377, http://dx.doi.org/10.1126/science.1252291.

[33] J.J. Martin, B.E. Fiore, R.M. Erb, Designing bioinspired composite reinforcement architectures via 3D magnetic printing, Nat. Commun. 6 (2015) 8641, http://dx.doi.org/10.1038/ncomms9641.

[34] Q. Ge, A.H. Sakhaei, H. Lee, C.K. Dunn, N.X. Fang, M.L. Dunn, Multimaterial 4D printing with tailorable shape memory polymers, Sci. Rep. 6 (2016) 31110, http://dx.doi.org/10.1038/srep31110.

[35] X. Zheng, J. Deotte, M.P. Alonso, G.R. Farquar, T.H. Weisgraber, S. Gemberling, et al., Design and optimization of a light-emitting diode projection micro-stereolithography three-dimensional manufacturing system, Rev. Sci. Instrum. 83 (12) (2012) 125001, http://dx.doi.org/10.1063/1.4769050.

[36] C. Sun, N. Fang, D.M. Wu, X. Zhang, Projection micro-stereolithography using digital micro-mirror dynamic mask, Sens. Actuators A: Phys. 121 (1) (2005) 113–120, http://dx.doi.org/10.1016/j.sna.2004.12.011.

[37] http://usglobalimages.stratasys.com/Main/Files/Material_Spec_Sheets/MSS_PJ_PJMaterialsDataSheet.pdf?v=635785205440671440.

[38] Evolution of material properties during free radical photopolymerization, J. Mech. Phys. Solids 112 (2018) 25–49, http://dx.doi.org/10.1016/j.jmps.2017.11.018.

[39] J.R. Tumbleston, D. Shirvanyants, N. Ermoshkin, et al., Continuous liquid interface production of 3D objects, Science 347 (6228) (2015) 1349–1352, http://dx.doi.org/10.1126/science.aaa2397.

[40] H. Gong, B.P. Bickham, A.T. Woolley, et al., Custom 3D printer and resin for 18 μm × 20 μm microfluidic flow channels, Lab Chip 17 (17) (2017) 2899–2909, http://dx.doi.org/10.1039/C7LC00644F.

[41] https://softroboticstoolkit.com/book/pneunets-mold-design-cad-tutorial.

Biographies

Lisen Ge received the B.E. degree in Engineering Structure Analysis and M.S. degree in Vehicle Operation Engineering from Southwest Jiaotong University, Chengdu, China, in 2013 and 2016, respectively. He is currently a Ph.D. candidate at School of Mechanical Engineering, Shanghai Jiao Tong University. His research is in the development of soft robotics.

Longteng Dong received the B.E. degree in mechanical engineering and automation from Jilin University, Changchun, China, in 2012. He worked as a mechanical engineer in a machine tool company from 2012 to 2015. He is currently a M.S. candidate at School of Mechanical Engineering, Shanghai Jiao Tong University. His research is in the development of 3D printing.

Dong Wang received the B.E. degree in mechanical engineering from Zhejiang University, China, in 2010 and the Ph.D. degree in Nanyang Technological University, Singapore, in 2015. He is currently working as a postdoc research fellow in Singapore University of Technology and Design, Singapore.

Qi Ge received his Ph.D. from University of Colorado at Boulder (CU Boulder), United States, in 2012 on experiments and modeling of shape memory polymers and composites. Currently, he is working as an assistant professor at Singapore University of Technology and Design (SUTD). Dr. Ge's research involves the development of multifunctional advanced manufacturing approaches, the development of functional printable materials, and the use of continuum mechanics coupled with multiphysics to understand multifunctional behaviors of active materials, and to develop computational tools to guide structure design with active materials. His primary areas of interest include: advanced manufacturing, additive manufacturing, functional materials, polymer science, continuum mechanics, and multiphysics. Prior to his appointment at SUTD, Dr. Ge did his postdoctoral research at SUTD, MIT and CU Boulder on development of high resolution multifunctional additive manufacturing system and 3D printing with active materials (4D printing). Dr. Ge has published more than 20 papers including papers published on high impact journals such as Science, Nature communicates, Advanced Materials, and he is recognized as one of the pioneers of the new 4D printing technology.

Guoying Gu received the B.E. degree (with honors) in electronic science and technology, and the Ph.D. degree (with honors) in mechatronic engineering from Shanghai Jiao Tong University, Shanghai, China, in 2006 and 2012, respectively. Dr. Gu was a Visiting Scholar at Concordia University, Montreal, QC, Canada, and National University of Singapore, Singapore. Supported by the Alexander von Humboldt Foundation, he was as a Humboldt Fellow at University of Oldenburg, Oldenburg, Germany. Since October 2012, he has worked at Shanghai Jiao Tong University, where he is currently appointed as an Associate Professor with School of Mechanical Engineering. His research interests include soft robotics, high-precision motion control, soft sensors and actuators. He is the author or co-author of over 60 publications, which have appeared in journals, as book chapters and in conference proceedings. Dr. Gu is a member of the IEEE and ASME. Now Dr. Gu serves as Associate Editor of International Journal of Advanced Robotic Systems. He has also served for several international conferences/symposiums as Chair, Associate Editor or Program Committee Member.